

Numerical investigations on breakage behaviour of granular materials under triaxial stresses

Lunlun Zhou ^{1a}, Xihua Chu ^{*1}, Xue Zhang ² and Yuanjie Xu ¹

¹ School of Civil Engineering, Wuhan University, Wuhan, 430072, China

² ARC Centre of Excellence for Geotechnical Science and Engineering, The University of Newcastle, NSW, 2308, Australia

(Received March 20, 2015, Revised December 25, 2015, Accepted June 08, 2016)

Abstract. The effect of particle breakage and intermediate principal stress ratio on the behaviour of crushable granular assemblies under true triaxial stress conditions is studied using the discrete element method. Numerical results show that the increase of intermediate principal stress ratio b ($b = (\sigma_2 - \sigma_3) / (\sigma_1 - \sigma_3)$) results in the increase of dilatancy at low confining pressures but the decrease of dilatancy at high confining pressures, which stems from the distinct increasing compaction caused by breakage with b . The influence of b on the evolution of the peak apparent friction angle is also weakened by particle breakage. For low relative breakage, the relationship between the peak apparent friction angle and b is close to the Lade-Duncan failure model, whereas it conforms to the Matsuoka-Nakai failure model for high relative breakage. In addition, the increasing tendency of relative breakage, calculated based on a fractal particle size distribution with the fractal dimension being 2.5, declines with the increasing confining pressure and axial strain, which implies the existence of an ultimate graduation. Finally, the relationship between particle breakage and plastic work is found to conform to a unique hyperbolic correlation regardless of the test conditions.

Keywords: particle breakage; discrete element method; intermediate principle stress ratio; particle size distribution; plastic work

1. Introduction

Particles breakage is commonly present in geotechnical engineering applications. Typical examples are the breakage of granules in penetrometer tests and high earth and rock-fill dams due to excessive stresses. For many weak-grained soils (such as decomposed granite soils, calcareous sands and volcanic ashes (Randolph *et al.* 1994, Bolton *et al.* 2008, Nakata *et al.* 1999), particle breakage occurs as well even under low stresses. Due to its considerable effect on the deformation and strength properties of granular materials, particle breakage continues to attract attention from researchers in both academia and industry (Lade *et al.* 1996, McDowell and Bolton 1998, Nakata *et al.* 2001a).

Previous studies showed that the likelihood of particle breakage chiefly depends on the characteristics of individual particles themselves and particle assemblies. On the (microscopic)

*Corresponding author, Professor, E-mail: Chuxh@whu.edu.cn

^a Ph.D. Student, E-mail: zhoulunlun@whu.edu.cn

individual particle level, it was reported that particles with lower mineral strength and larger angularity are more likely to crush, and the increasing individual particle size may also enhance the possibility of the breakage because a larger particle has a relatively higher probability of containing a flaw (Lade *et al.* 1996, McDowell and Bolton 1998). On the (macroscopic) assembly level, it was observed that particle assemblies with well gradation and high initial density are more difficult to break down (Lade *et al.* 1996, McDowell and Bolton 1998, Nakata *et al.* 2001a, b). Lade *et al.* (1996) explained this based on the fact that the increasing coordination number surrounding each particle of the assembly decreases the average contact stress.

Regarding the effect of external loadings, the experimental tests conducted by Lade *et al.* (1996) and Tarantino and Hyde (2005) exhibited that the amount of particle crushing is increased by the confining stress magnitude; however, when the confining stress magnitude is sufficiently large the amount becomes constant. Ezaoui *et al.* (2011) and Casini *et al.* (2013) observed that, compared to that in a shearing stress path, in an isotropic stress path a higher pressure must be applied to create breakage in granular materials. In addition, it was reported that a shearing stress path creates finer particles than these produced in an isotropic stress path. Although the breakage behaviour of granular materials has been studied extensively in various laboratory tests (Lade *et al.* 1996, Tarantino and Hyde 2005, Ezaoui *et al.* 2011, Casini *et al.* 2013), such as uniaxial compression tests, isotropic compression tests, and conventional triaxial tests, the allowable stress paths applied in these tests are all under axisymmetric conditions. There are few works devoted to investigating the breakage behaviour under true triaxial stress conditions defined by the intermediate principal stress parameter b ($b = (\sigma_2 - \sigma_3) / (\sigma_1 - \sigma_3)$) which is believed to have a significantly influence on the strength characteristic of granular materials (Wang and Lade 2006, Sun *et al.* 2008, O'Sullivan *et al.* 2013, Huang *et al.* 2014, Ng 2004). Furthermore, some inherent difficulties in laboratory tests, such as the controlling of the initial fabric of samples and the extracting of particle-level information, do limit their application for investigating the breakage behaviour of particle assemblies.

The discrete element method (DEM), as a numerical method that can overcome these difficulties in experimental tests, has been adopted to investigate the particle breakage behaviour extensively (Robertson 2000, McDowell and Harireche 2002a, b, Cheng *et al.* 2003, 2004, Bolton *et al.* 2008, Wang and Yan 2012, 2013, Chu and Li 2006, Zhou and Chu 2014). In the DEM simulation, one possible way to capture the particle breakage process is to model crushable particles as numerical agglomerates composed of bonded elementary balls, which was originally proposed by Robertson (2000) who successfully reproduced the Weibull statistics of particle fracture strength by introducing probabilistic flaws through the random removal of a certain portion of elementary balls. Inspired by Robertson's work (Robertson 2000), McDowell and Harireche (2002a, b) suggested a procedure of creating crushable agglomerates with different sizes to reproduce the particle size effect on particle fracture strength. Cheng *et al.* (2003, 2004) simulated silica sand particles with real statistical strengths, and the numerical triaxial tests on the assembly of agglomerates reproduced the plastic behaviour of real sands. Bolton *et al.* (2008) provided a discussion on the effect of micro-parameters, e.g., coordination number, fabric tensor, and energy, on the macroscopic behaviour of crushable soils based on DEM triaxial tests. Wang and Yan (2012, 2013) presented a detailed investigation of the effect of particle breakage on the shear localization, shear failure behaviour and energy dissipation of crushable materials. Chu and Li (2006) suggested a hierarchical crushable model based on the DEM, and investigated the influence of breakage on the macro-micro mechanical behaviour of granular materials (Zhou and Chu 2014).

In this study, the effect of test conditions, such as confining pressure level and stress paths, on the evolution of particle breakage is investigated numerically using the discrete element simulation. A series of drained triaxial tests, including triaxial compression tests and constant σ_3 true triaxial tests, are carried out on a numerical specimen composed of ellipsoidal crushable agglomerates. The breakage mechanism of crushable granular materials under true triaxial stress conditions is investigated through analyzing the stress-strain characteristics, the evolution of particle size distribution and relative breakage, and the relationship between the breakage and the plastic work received in the test.

2. Simulation method

2.1 Single particle crushing simulation

The effective simulation of single particle crushing is the precondition for achieving a realistic simulation of breakage behaviour in crushable granular assemblies. Previous experimental works (Nakata *et al.* 2001a, McDowell and Bolton 1998) indicated that Weibull’s statistical distribution can characterise the individual particle fracture strength well. The survival probability $P_s(d)$ of an individual particle of size d under platen compressions is given by (Weibull 1951)

$$P_s(d) = \exp\left[-(\sigma/\sigma_0)^m\right] \tag{1}$$

where σ is the induced tensile stress calculated by $\sigma = F/d^2$ (F is the diametrical force between two flat platens), σ_0 is the characteristic tensile stress (37% or $1/e$ of the tested particles survive when $\sigma = \sigma_0$, $e \approx 2.71828$), and m is the Weibull modulus.

In this study, the commercial software PFC3D (Itasca Consulting Group, Inc. 2008) is used to carry out the discrete element simulation. Ellipsoidal, rather than spherical, agglomerates are chosen to represent the crushable soil particles. All the agglomerates are the same spheroid with a pair of equal minor axes of 1.0 mm and a major axis of 1.2 mm, and are composed of a certain number of bonded elementary balls with diameters being 0.2 mm. Table 1 gives the shape parameters of the ellipsoid, where a typical ellipsoidal agglomerate is also illustrated. To create the agglomerate, an initial set of 73 elementary balls with a smaller diameter are first generated randomly in an ellipsoidal container of the same dimension as the ellipsoidal agglomerate. The balls are then expanded gradually to their final diameter (0.2 mm) and the system is cycled to equilibrium so as to reduce unwanted overlaps. Afterwards, parallel bonds are installed at all the

Table 1 Shape and size parameters of crushable agglomerates

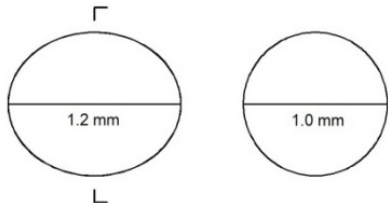
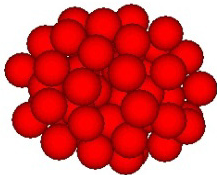
Number of balls	Agglomerate size/mm	Typical agglomerate
57		

Table 2 Micro parameters of elementary balls and parallel bond used in DEM simulation

Diameter of element ball: mm	0.2
Density of ball: kg/m ³	2650
Normal and shear stiffness of ball: N/m	2×10 ⁶
Friction coefficient of ball	0.5
Normal and shear parallel bond strength: N/m ²	1.0×10 ⁹
Normal and shear parallel bond stiffness: N/m ²	5×10 ¹⁴
Ratio of parallel bond radius to ball radius	0.5

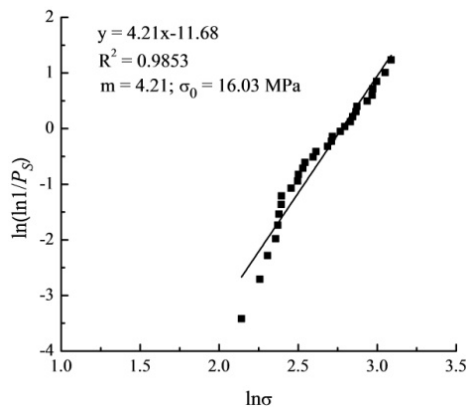


Fig. 1 Weibull probability plot of crushable agglomerates from platen compression tests

contacts between elementary balls to form the bonded agglomerate. The advantage of the parallel bond model over the contact bond model, which was widely used in previous DEM studies (Robertson 2000, McDowell and Harireche 2002a, b, Cheng *et al.* 2003, 2004, Bolton *et al.* 2008), is that it is able to transmit a rotational resistance with a finite piece of cement (Itasca Consulting Group, Inc. 2008). Wang and Yan (2012, 2013) indicated that the absence of this rotational resistance will frequently lead to the absence of a clear, visible physical fracture of agglomerate, although a distinct peak stress indicating the major splitting of the agglomerate can usually be observed. Hence, the parallel bond model is adopted to avoid this unrealistic behavior in this study. The parameters of elementary balls and parallel bond model are sourced from those used by Wang and Yan (2012, 2013) which are shown in Table 2. In order to provide a statistical variation of the fracture strength, each bonded agglomerate is subjected to a random removal of about 20% elementary balls. As a result, the number of balls in the final agglomerate is reduced to 57.

Fig. 1 shows the Weibull probability curve of thirty random agglomerates, which are numerically crushed in a platen compression test. The survival probability P_S is calculated using the mean rank position proposed by Davidge (1979). According to Davidge (1979), if the number of tests is represented by N , the survival probabilities of agglomerates under increasing stresses are $N / (N + 1)$, $(N - 1) / (N + 1)$, ..., $1 / (N + 1)$. As shown in Figure 1, the relationship between the survival probability and the corresponding fracture stress obtained from the numerical simulation is comparable to the Weibull's distribution (the solid line) with the modulus $m = 4.21$ and fracture strength $\sigma_0 = 16.03$ MPa.

2.2 Specimen preparation and testing

The initial dimension of the three-dimensional DEM specimen is $12 \times 8 \times 8$ mm. It consists of 696 ellipsoidal agglomerates as shown in Table 1 (a total of 39672 elementary balls). To reduce the computational cost, the number of agglomerates utilised in the simulation is much less than these in a real specimen. Nevertheless, it is believed that the number of agglomerates used here is sufficiently large to produce the behaviour of the specimen in a real experimental test. Indeed, Cheng *et al.* (2003, 2004) has successfully replicated the complex behaviour of real crushable sands, in relation to their strength, dilatancy and critical states, with only 389 numerical agglomerates using 17274 spheres (which is even much less than that in our simulations). Moreover, the following results also validate the number of agglomerates used in our simulations.

The triaxial box is composed of six rigid frictionless walls. To generate the specimen, smaller balls are first produced within the triaxial box and then expanded to the final diameter, which is equal to the length of major axis of the ellipsoidal agglomerate (1.2 mm). During this process, the shear stiffness and friction coefficient are set to be zero, and the target void ratio is assigned to be 0.25. After the diameter of balls expands to the required value (1.2 mm), they are replaced by randomly rotated ellipsoidal agglomerates and the system is cycled to pursue the force equilibrium.

Fig. 2 illustrates the typical DEM specimen generated by the above described procedure. Two sets of drained tests are performed numerically based on the generated specimen. In the first set, conventional triaxial compression tests are conducted under different confining pressures, namely, $\sigma_3 = 0.1, 0.4, 0.8, 1.6, 2.4, 5.0,$ and 8.0 MPa. In the second set, true triaxial tests are focused on with σ_3 being constant at 0.1 and 2.4 MPa, respectively, and the intermediate principal stress parameter b being $0.0, 0.25, 0.5, 0.75,$ and 1.0 . In the two special cases of $b = 0$ ($\sigma_2 = \sigma_3$) and $b = 1$ ($\sigma_1 = \sigma_2$), the tests represent the conventional triaxial compression and extension tests, respectively.

Before subjected to shear deformation, the specimen is first consolidated isotropically with the confining pressures σ_3 until the equilibrium is achieved. After the consolidation under $\sigma_3 = 0.1$ MPa, the void ratio of specimen, calculated by using the solid volume as the total volume of the agglomerates, is 2.03 (the approximate value of 2.1 used by Cheng *et al.* (2003)). Then the vertical strain on the compressed specimen is increased to induce shear deformation. During this phase, the top and bottom walls move towards each other at a constant speed of 0.05 mm/s, and the speed of lateral walls are controlled by a servo-control algorithm to keep the confining stress constant in conventional triaxial compression tests or keep the minor principal stress and b value constant in true triaxial tests. The principal stress direction is defined as shown in Fig. 2.

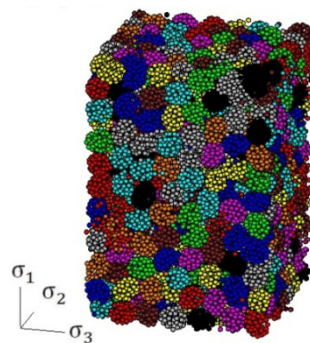


Fig. 2 DEM specimen of 696 crushable agglomerates

3. Simulation results and analysis

3.1 Stress-Strain Characteristics

Fig. 3 shows the curves of the deviatoric stress ratio q/p ($q = \sigma_1 - \sigma_3$, $p = (\sigma_1 + \sigma_2 + \sigma_3)/3$) and the volumetric strain against the axial strain from the conventional triaxial compression tests. At low confining pressure levels, the numerical specimen exhibits evident dilatancy. More specifically, for $\sigma_3 = 0.1$ MPa the volume of the specimen contracts slightly at first, which then dilates significantly and reaches a stable critical state when the strain is sufficiently large. In addition, post-peak strain softening behaviour is also observed as shown in Figure 3. Under high confining pressures, continuous volumetric contraction runs through the whole tests, attributed to the fact that more particles break into smaller ones which consequently fill the original voids of specimen. In the extreme cases, e.g., $\sigma_3 = 5.0$ and $\sigma_3 = 9.0$ MPa, the total volume decreases almost linearly as the axial strain increases. Accompanying the continuous volumetric contraction at high confining pressures, the corresponding stress ratio curves show distinct strain hardening characteristic. As the degree of particle breakage increases with increasing confining pressure, the peak stress ratio and dilatancy of specimen decrease gradually, and the stress-strain behaviour transforms gradually from strain softening to strain hardening. Based on the observation in our simulations, it can be concluded that the particle breakage weakens the dilatancy and strain softening characteristic of granular materials.

The curves of deviatoric stress ratio q/p and volumetric strain versus axial strain obtained from the true triaxial tests under confining pressures $\sigma_3 = 0.1$ and 2.4 MPa are plotted in Fig. 4 and 5, respectively. It can be seen that for both confining pressures the peak stress ratio q/p reduces as b increases. All curves of the volume change at $\sigma_3 = 0.1$ MPa turn from contraction to dilation in the range of axial strain $\varepsilon_1 = 5\% \sim 10\%$ and the corresponding values of axial strain at the turning points decrease with increasing b which means the dilatancy of the specimen increases with b . The volumetric deformation is the result of competition between two contrasting deformation mechanisms, namely, shear-induced dilation caused by particle rearrangement and shear-induced compression caused by particle breakage (Wang and Yan 2013). The dilation caused by particle rearrangement increases with the increasing external pressures (σ_1, σ_2) as b increases. On the other

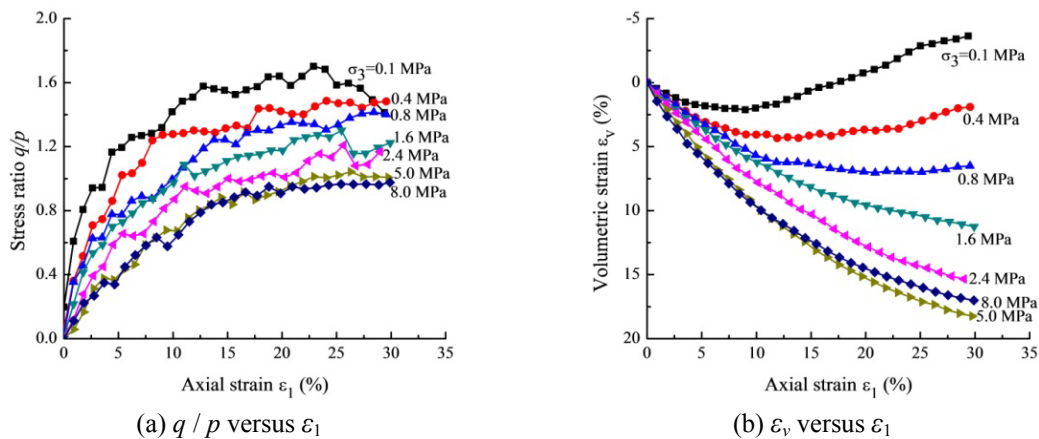


Fig. 3 Stress-strain relations from conventional triaxial compression tests

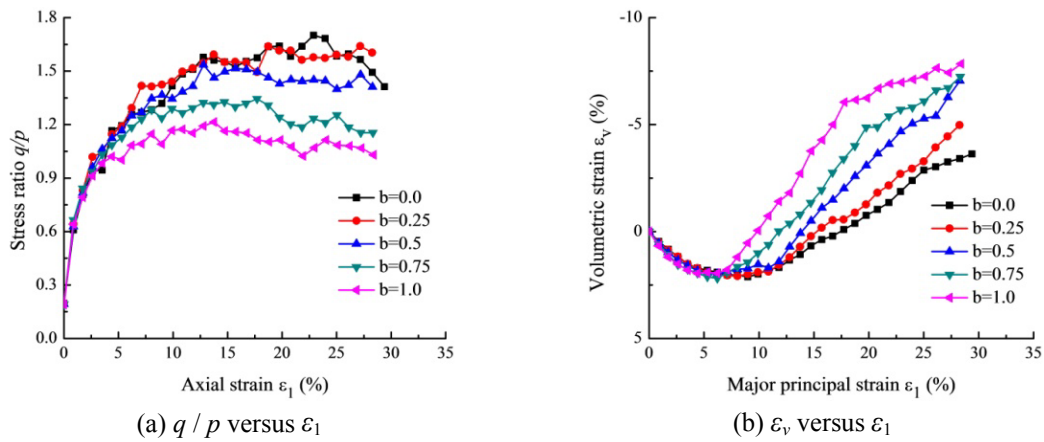


Fig. 4 Stress-strain relations from true triaxial tests ($\sigma_3 = 0.1$ MPa)

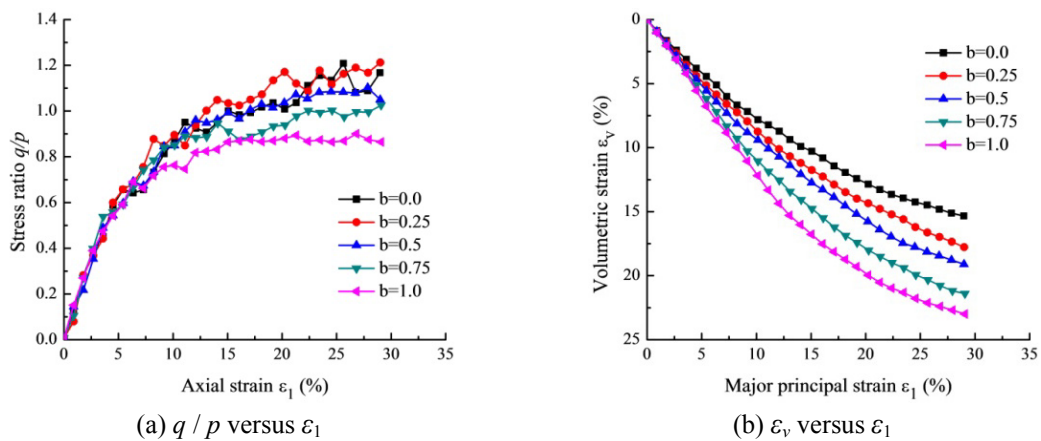


Fig. 5 Stress-strain relations from true triaxial tests ($\sigma_3 = 2.4$ MPa)

hand, compression caused by particle breakage does not increase significantly, since the amount of particle breakage increases slightly with increasing b at $\sigma_3 = 0.1$ MPa. The dilation caused by particle rearrangement is the dominant mechanism. In contrast, the volumetric strain responses keep contracting for all b values tested at $\sigma_3 = 2.4$ MPa, and the contraction increases with increasing b . This is because particle breakage has become an important factor in the volumetric deformation and the compaction caused by particle breakage increases significantly with increasing b at $\sigma_3 = 2.4$ MPa.

The evolutions of the intermediate and minor principal strains (ϵ_2, ϵ_3) against the major principal strain ϵ_1 from the true triaxial tests under $\sigma_3 = 0.1$ and 2.4 MPa are shown in Figs. 6 and 7, respectively. The relationships between principal strains are similar regardless of the imposed confining pressure. The intermediate principal strain turns from expansion to contraction progressively as b increases. For $b \leq 0.25$, the response is extensive, otherwise it is compressive. The minor principal strain exhibits expansion in all cases of b and the expansion in this principal direction increases with the value of b .

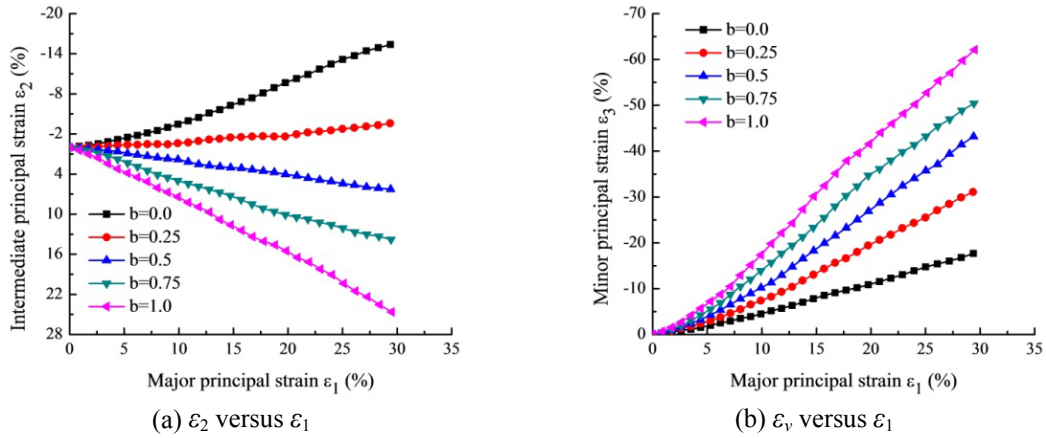


Fig. 6 Relations between principal strains from true triaxial tests ($\sigma_3 = 0.1$ MPa)

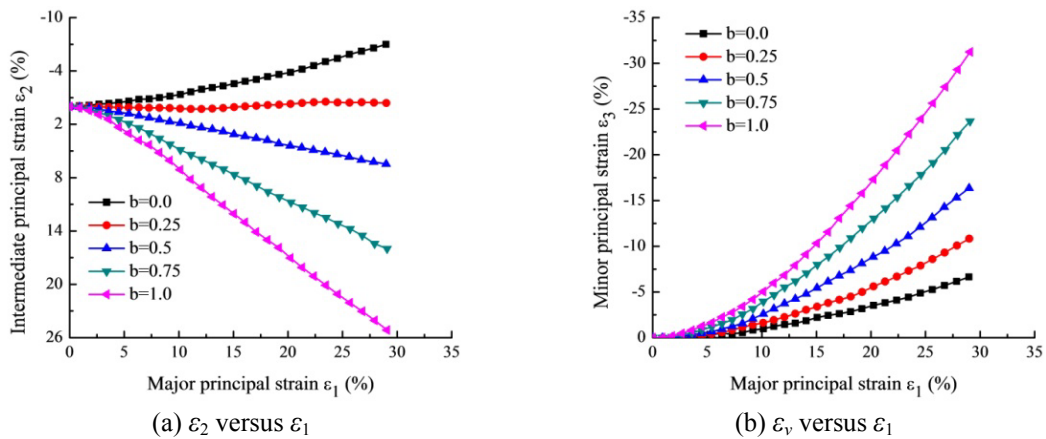


Fig. 7 Relations between principal strains from true triaxial tests ($\sigma_3 = 2.4$ MPa)

Fig. 8(a) shows the relationship between the peak apparent friction angle, defined as the maximum $\phi = \sin^{-1}[(\sigma_1 - \sigma_3) / (\sigma_1 + \sigma_3)]$ at the peak point of the stress-strain curve in Fig. 3(a), and the corresponding confining pressure from the conventional triaxial tests. The peak friction angle decreases with increasing confining pressure, which conforms perfectly to the logarithmic relationship suggested by Duncan *et al.* (1980): $\phi = \phi_0 - \Delta\phi \lg(\sigma_3 / p_a)$, where p_a is the atmospheric pressure, ϕ_0 is the friction angle corresponding to $\sigma_3 = p_a$, and $\Delta\phi$ is the curve-fit parameter reflecting the reduction of friction angle ($\phi_0 = 41.83^\circ$ and $\Delta\phi = 8.69^\circ$ in this study). The value of peak friction angle at $\sigma_3 = 8.0$ MPa in this simulation is 25.21° , which is slightly lower than the actual value of sands (Budhu 2008). The lower friction angle is the result of the weaker interlocking between particles in the numerical specimen, in which there are a high percentage of spherical particles produced by the breakage of irregular particles at high pressure level.

The relationships between the peak friction angle, at the peak point of the stress-strain curve in Figs. 4(a) and 5(a), and b value from all true triaxial tests under $\sigma_3 = 0.1$ and 2.4 MPa are depicted in Figs. 8(b) and 8(c), respectively. The predicted friction angles based on the Lade-Duncan (1975)

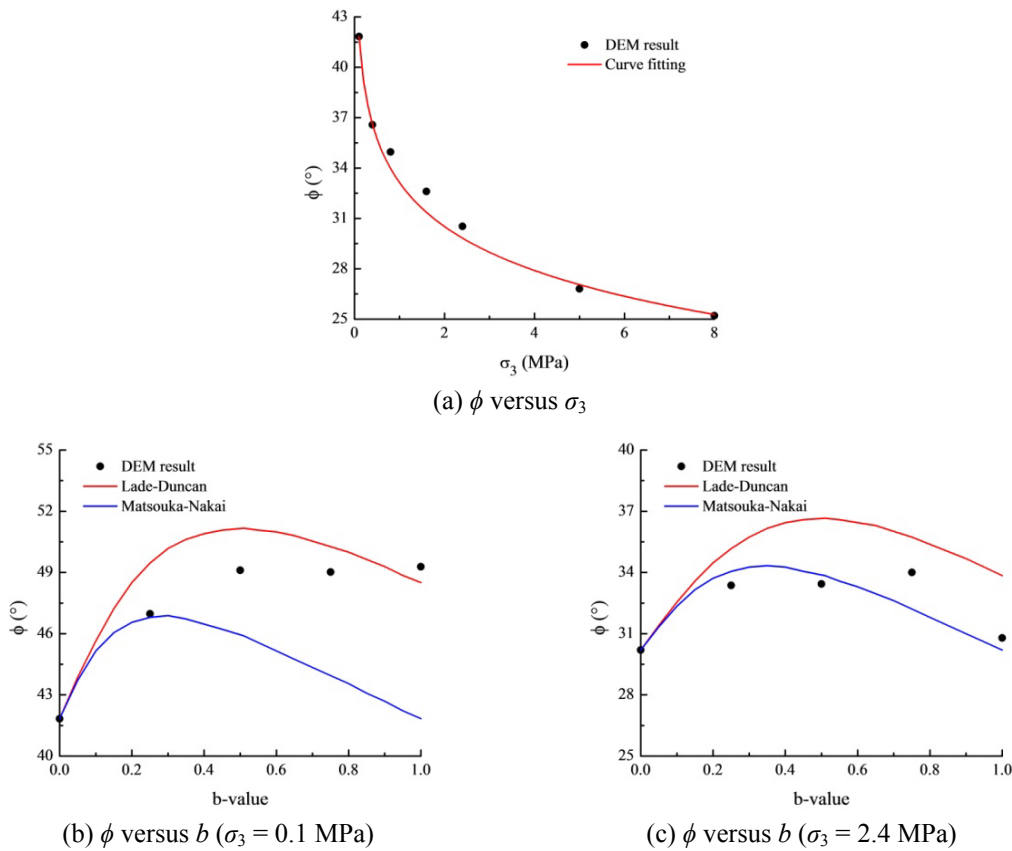


Fig. 8 Relations between friction angle, confining pressure and parameter b

and Matsuoka-Nakai (1978) failure models are also plotted for comparison. For $\sigma_3 = 0.1$ MPa, the peak friction angle increases continuously with the value of b until $b = 0.5$, after which the rate of the increase reduces significantly and the peak friction angle remains practically constant as b increases. The relationship obtained at $\sigma_3 = 0.1$ MPa is much closer to the Lade-Duncan failure model which predicts a higher friction angle. At confining pressure $\sigma_3 = 2.4$ MPa, the peak friction angle first increases with b ; after $b = 0.25$, it increases slowly until $b = 0.75$ and then decreases rapidly. Such result conforms to the Matsuoka-Nakai failure model with lower prediction. O'Sullivan *et al.* (2013) demonstrated that the variation in lateral support to the strong force chains plays a central role explaining the sensitivity of peak friction angle to b . The variation of force chains with b changes the contact stress of particles, which directly affects the amount of particle breakage. The difference of effects of b value on the peak angle for the two confining pressures is probably because that the amount of particle breakage increases with the value of b considerably at $\sigma_3 = 2.4$ MPa, but slightly at $\sigma_3 = 0.1$ MPa; thus in the case of $\sigma_3 = 2.4$ MPa particle breakage weakens the influence of b on the evolution of peak apparent friction angle to some extent.

3.2 Quantification of particle breakage

Several different particle breakage indices have been proposed to quantify the amount of

particle breakage (Lade *et al.* 1996, Tarantino and Hyde 2005, Hardin 1985). Among them, the most widely used particle breakage factor is the one developed by Hardin (1985). Hardin (1985), based on the general changes in particle size distribution, defined the relative breakage as the ratio of total breakage divided by the potential breakage

$$B_r = \frac{B_t}{B_p} \quad (2)$$

where B_t is the total breakage represented by the area between the current particle size distribution curve and the original particle size distribution curve, the breakage potential B_p represents the total possible change in particle size distribution and is defined as the area between the original particle size distribution curve and a cut-off value of silt particle size of 0.074 mm, which implies that all particles will eventually become finer than this cut-off value (0.074 mm). Despite its widely application, Hardin's implication conflicts with the results obtained from several experimental tests (Lade *et al.* 1996, McDowell and Bolton 1998, Zhang *et al.* 2013) that the effect of particle breakage is to increase the proportion of fines without significantly changing the size of the largest particles, and the particle size distribution after breakage gradually tends to be an ultimate self-similar, fractal distribution. Consequently, Einav (2007) adjusted the definition of relative breakage to the relative position of the current particle size distribution from the original particle size distribution and the ultimate fractal particle size distribution. More specifically, for a fractal particle size distribution, the number of particles which have a size Δ greater than size d is expressed by

$$N(\Delta > d) = Ad^{-D} \quad (3)$$

where A is a constant coefficient and D is the fractal dimension. While the number of particles in a fraction is

$$dN(\Delta) = DAd^{-D-1}d\Delta \quad (4)$$

The cumulative particle size distribution is equal to

$$p_d = \frac{\int_0^d s\rho_s\Delta^3 dN(\Delta)}{\int_0^{d_M} s\rho_s\Delta^3 dN(\Delta)} \quad (5)$$

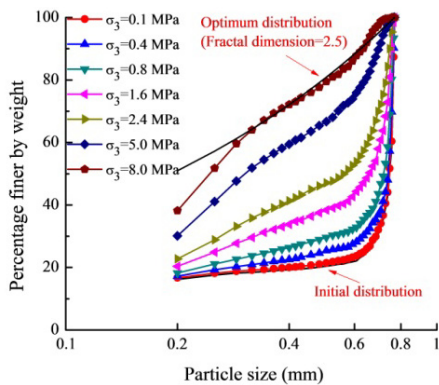
where s is a shape factor, ρ_s is the particle density, and d_M is the largest particle size in the sample. Substituting Eq. (4) into Eq. (5), the following expression for the fractal particle size distribution is obtained

$$p_d = (d/d_M)^{3-D} \quad (6)$$

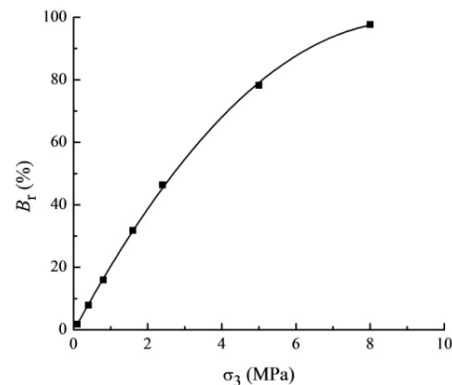
The final particle size distributions from all the conventional compression tests are plotted in Fig. 9(a), where the fractal size distribution with $D = 2.5$ and the initial gradation are also illustrated for comparison. The representative particle size of the agglomerate is defined as the diameter of a sphere, the volume of which is equal to the solid volume of an individual agglomerate. Initially, because particle breakage occurs during the specimen preparation, there are

a percentage of broken fragments in the initial gradation. It is clearly observed that particle size distribution gradually shifts toward a more well-graded distribution as the confining stress increases. The largest size of particles remains unchanged and the smallest size is restricted by the size of elementary ball. The final particle size distribution in this study tends to the fractal size distribution with the fractal dimension of 2.5, which is in accordance with the results obtained by McDowell and Bolton (1998) and Coop *et al.* (2004). McDowell and Bolton (1998) found that the fractal dimension for uniaxial compression is generally around 2.5 for many granular materials subjected to pure crushing, and the value for shearing identified by Coop *et al.* (2004) is 2.57 (slightly higher than 2.50).

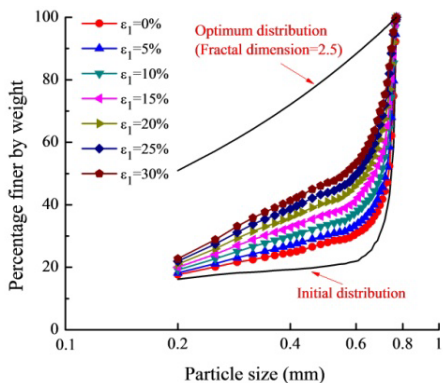
Coop *et al.* (2004) also showed that the ultimate particle size distribution in shearing strongly depends on the stress level, and the strains taken to reach an ultimate distribution are very much higher than that could be reached in a triaxial test. For simplicity, within the range of the testing confining pressure level and the applied axial strain in the current study, the fractal particle size distribution with $D = 2.5$ is artificially selected as the ultimate distribution to calculate the relative breakage B_r , based on Einav's modified measure (Einav 2007). This does lead to a difference in the value calculated, but the evolution of relative breakage is not affected.



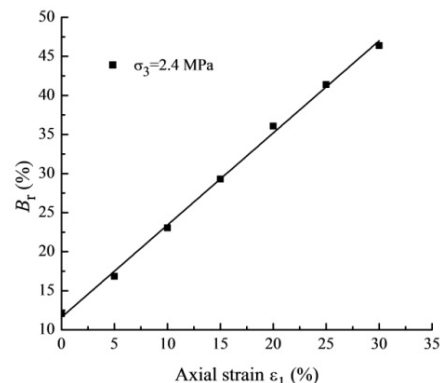
(a) Comparison of final particle size distribution



(b) Evolution of relative breakage with increasing σ_3

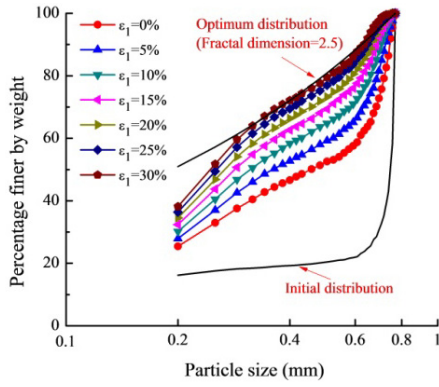


(c) Evolution of particle size distribution with increasing ϵ_1 ($\sigma_3 = 2.4$ MPa)

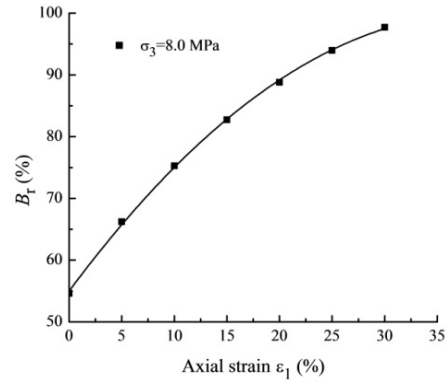


(d) Evolution of relative breakage with increasing ϵ_1 ($\sigma_3 = 2.4$ MPa)

Fig. 9 Particle size distributions and relative breakage from conventional triaxial compression tests

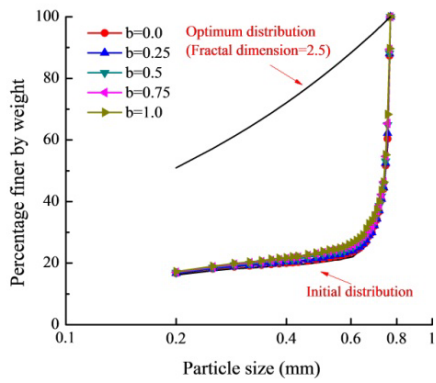


(e) Evolution of particle size distribution with increasing ϵ_1 ($\sigma_3 = 8.0$ MPa)

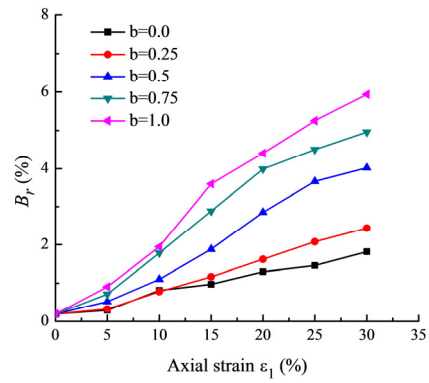


(f) Evolution of relative breakage with increasing ϵ_1 ($\sigma_3 = 8.0$ MPa)

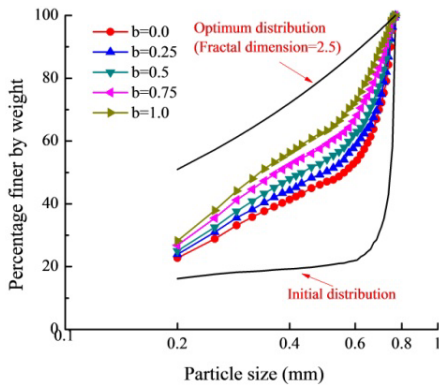
Fig. 9 Continued



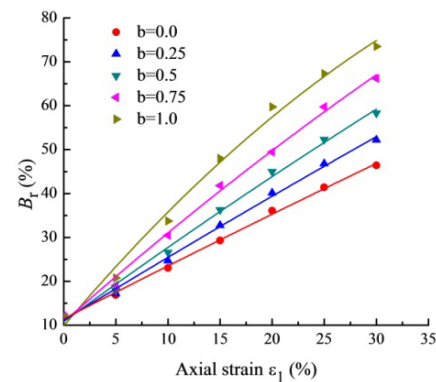
(a) Comparison of final particle size distribution ($\sigma_3 = 0.1$ MPa)



(b) Evolution of relative breakage with ϵ_1 ($\sigma_3 = 0.1$ MPa)



(c) Comparison of final particle size distribution ($\sigma_3 = 2.4$ MPa)



(d) Evolution of relative breakage with increasing ϵ_1 ($\sigma_3 = 2.4$ MPa)

Fig. 10 Particle size distributions and relative breakage from true triaxial tests

The relationship between the relative breakage B_r , calculated based on the grading curves in Fig. 9(a), and the corresponding confining pressure is plotted in Fig. 9(b). It can be seen that the relative breakage increases with the increasing confining pressure, but the rate of increase decreases gradually as confining pressure increases. This observation implies that particle breakage will eventually stabilize and an ultimate distribution exists as the confining pressure is sufficiently large. Figs. 9(c)-9(f) show the evolution of particle size distribution and the corresponding relative breakage with the increasing axial strain from the conventional triaxial compression tests for $\sigma_3 = 2.4$ and 8.0 MPa, respectively. For $\sigma_3 = 2.4$ MPa, particle size distribution is still far away from the ultimate distribution, the relative breakage increases linearly with the increasing strain. By contrast, the rate of increase of the relative breakage gradually declines with increasing strain at $\sigma_3 = 8.0$ MPa, where particle size distribution is already close to the ultimate distribution. Since we calculate the relative breakage with an ultimate fractal dimension of 2.5, the value of relative breakage in Figs. 9(b) and 9(f) would reach or go above 100% if the confining pressure and axial strain continue to increase. However, the obvious reduction of the increase rate of the relative breakage means that the ultimate distribution is near, and it is appropriate to calculate the relative breakage using fractal distribution with $D = 2.5$ within the range of the pressure level and the applied strain in this study.

Fig. 10 shows the final particle size distribution from all the true triaxial tests and the evolution of corresponding relative breakage with increasing axial strain. It can be seen that the particle size distribution has no significant change at $\sigma_3 = 0.1$ MPa, and the corresponding relative breakage for all b values are very small with the maximum of 5.9%. At $\sigma_3 = 2.4$ MPa, the particle size distribution shifts towards the final particle distribution obviously, this is a result of the significant increase of particle breakage as b increases. Both relative breakage at $\sigma_3 = 0.1$ MPa and $\sigma_3 = 2.4$ MPa are increasing linearly with axial strain for all b values, and the rate of breakage increase rises significantly with the increasing value of b , because particle size distributions are still far away from the ultimate distribution.

3.2 Dependence of breakage on plastic work

As Lade *et al.* (1996) mentioned, particle breakage of granular materials is directly related to the total energy input for a unit volume of specimen. In this section, we investigate the relationship between the relative breakage and the plastic work during the tests. The plastic work W_p , as the irrecoverable part of total input energy, is defined by

$$W_p = W_T - W_E \quad (7)$$

where W_T is the total energy input per unit volume of a specimen, W_E is the recoverable part of input energy.

The total energy input per unit volume of a specimen in a triaxial test is defined by

$$W_T = \int q \cdot \delta \varepsilon_s + \int p \cdot \delta \varepsilon_v = \int \sigma_1 \cdot \delta \varepsilon_1 + \int \sigma_2 \cdot \delta \varepsilon_2 + \int \sigma_3 \cdot \delta \varepsilon_3 \quad (8)$$

where $\delta \varepsilon_v = \delta \varepsilon_1 + \delta \varepsilon_2 + \delta \varepsilon_3$ and $\delta \varepsilon_q = \delta \varepsilon_1 - \delta \varepsilon_v / 3$ are the increments of volumetric and deviatoric strains, respectively. For a conventional triaxial stress state, the relations $\sigma_2 = \sigma_3$ and $\delta \varepsilon_2 = \delta \varepsilon_3$ hold.

The recoverable part W_E is defined by

$$W_E = \int (q \cdot \delta \varepsilon_s)_E + \int (p \cdot \delta \varepsilon_v)_E \tag{9}$$

where $\int (q \cdot \delta \varepsilon_s)_E$ and $\int (p \cdot \delta \varepsilon_v)_E$ are the recoverable part of energy caused by deviatoric stress and mean normal stress, respectively. Assuming the recoverable part of input energy caused by deviatoric stress $\int (q \cdot \delta \varepsilon_s)_E = 0$. And the recoverable part of energy caused by mean normal stress should be much less than the plastic work during the tests. Therefore, the recoverable part W_E is neglected in the actual calculation process of plastic work.

Figs. 11(a) and (b) present the relationships of the plastic work and the relative breakage from the conventional triaxial compression tests and true triaxial tests, respectively. The plastic work is calculated from the beginning of isotropic confining compression to the point where we extract data. It can be observed that the particle breakage increases with the increasing plastic work, but the rate of increasing breakage is decreasing gradually with the accumulation of plastic work. This indicates that as particle breakage increases gradually and particle size distribution gets closer to the ultimate distribution, it needs more plastic work to produce the same amount of particle breakage. This result is consistent with the recognition that the limitation of particle breakage exists.

Lade *et al.* (1996) has suggested that the relationship of particle breakage factor B_{10} to the energy input in triaxial tests is as

$$B_{10} = \frac{W_T}{\alpha + \beta W_T} \tag{10}$$

where α and β are the hyperbolic curve-fit parameters, the theoretical value of β is unity. Referring to this equation, all of the data points from the numerical tests are fitted in Fig. 12. In this study, the curve-fit parameters $\alpha = 4.23$ and $\beta = 0.5$. Because the fractal distribution with $D = 2.5$ is artificially selected as the ultimate distribution to calculate relative breakage, the β value of our numerical simulation is less than its theoretical value. It is clear in Fig. 12 that there is a unique hyperbolic correlation between the plastic work and the relative breakage independent of the test

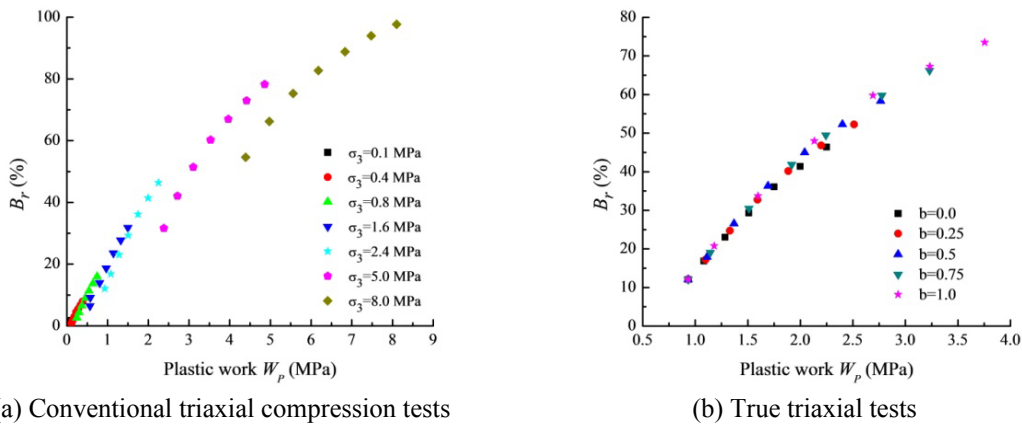


Fig. 11 Relations between relative breakage B_r and plastic work W_p

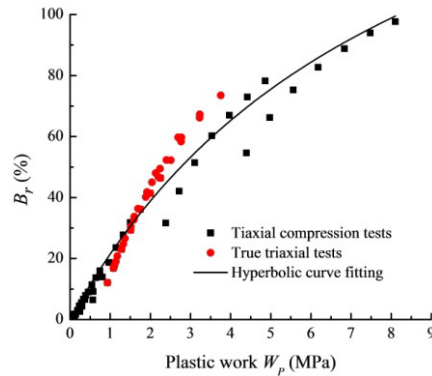


Fig. 12 Hyperbolic relationship between relative breakage B_r and plastic work W_p

conditions, including the confining pressure and stress path. This numerical result is in good agreement with the experimental result of Lade *et al.* (1996). This is probably due to the fact that the specimen used in our simulation is almost isotropic, which results in that the proportional relationship between energy dissipation, such as breakage dissipation, fractional dissipation and damping dissipation, and the plastic work may be insensitive to these test conditions. Further works from the microscopic point of view, such as energy dissipation, anisotropy of fabric and force chains, are required to investigate the possible micro-mechanical mechanism of this macro-mechanical behaviour.

4. Conclusions

This paper illustrates the results of a DEM numerical investigation of the mechanical behaviour of crushable granular materials under true triaxial stress conditions. More specifically, the shear strength, the deformation behaviour, the evolution of particle size distribution and the relative breakage, as well as the relationship between the relative breakage and the plastic work received during tests are investigated. A series of conventional triaxial compression tests and true triaxial tests are conducted on a numerical specimen composed of ellipsoidal crushable agglomerates. The fracture strength of the numerical particles satisfies the Weibull's statistical distribution well. The following conclusions are derived from the numerical tests:

- (1) As the confining pressure increases, the dilatancy of the specimen decreases gradually and the stress-strain behaviour transforms gradually from strain softening to strain hardening with increasing particle breakage. Particle breakage weakens the dilatancy and the strain softening characteristic of granular materials notably.
- (2) Particle breakage considerably affects the evolution of dilatancy of specimen with b value. At low confining pressure, the dilatancy of the specimen increases with the increase of b whereas it decreases at high confining pressure which stems from the distinct increase of breakage in this case.
- (3) The peak apparent friction angle decreases monotonically with the increasing confining pressure, which conforms to a logarithmic relationship. The relationship between the peak apparent friction angle and b for low relative breakage is closer to the Lade-Duncan failure

model with higher prediction, but conforms to the Matsuoka-Nakai failure model with lower prediction for high relative breakage. This is because particle breakage weakens the influence of b on the evolution of the peak friction angle to some extent.

- (4) The distribution of particle size gradually tends to be a fractal one with $D = 2.5$. When the distribution is close to the ultimate value, the increase rate of breakage decreases with the confining pressure and axial strain. Relative breakage for b at different values increases linearly with the axial strain, and the rate of the increase also grows with the value of b .
- (5) Particle breakage is found to have a unique hyperbolic correlation with the plastic work received during the numerical tests, which is independent of the test conditions. Such independence may result from the fact that the proportional relationship of the energy dissipation (such as breakage dissipation, fractional dissipation, and damping dissipation) and the plastic work are insensitive to the test conditions for isotropic specimens. Further works from the microscopic point of view are required to investigate the possible micro-mechanical origins of this macro-mechanical behaviour.

Acknowledgments

The authors are pleased to acknowledge the support of this work by the National Natural Science Foundation of China through contract/grant number 10802060 and 11172216 and the Natural Key Basic Research and Development Program of China (973 Program) through contract/grant numbers 2010CB731502.

References

- Bolton, M.D., Nakata, Y. and Cheng, Y.P. (2008), "Micro- and macro-mechanical behaviour of DEM crushable materials", *Geotechnique*, **58**(6), 471-480.
- Budhu, M. (2008), *Soil Mechanics and Foundations*, Wiley, New York, NY, USA.
- Casini, F., Viggiani, G.M.B. and Springman, S.M. (2013), "Breakage of an artificial crushable material under loading", *Granul. Matter.*, **15**(5), 661-673.
- Cheng, Y.P., Nakata, Y. and Bolton, M.D. (2003), "Distinct element simulation of crushable soil", *Geotechnique*, **53**(7), 633-641.
- Cheng, Y.P., Bolton, M.D. and Nakata, Y. (2004), "Crushing and plastic deformation of soils simulated using DEM", *Geotechnique*, **54**(2), 131-141.
- Chu, X.H. and Li, X.K. (2006), "Hierarchical multi-scale discrete particle model and crushing simulation", *J. Dalian. Univ. Techno.*, **46**, 319-326. [In Chinese]
- Coop, M.R., Sorensen, K.K., Bodas, Freitas, T. and Georgoutsos, G. (2004), "Particle breakage during shearing of a carbonate sand", *Geotechnique*, **54**(3), 157-163.
- Davidge, R.W. (1979), *Mechanical Behaviour of Ceramics*, University of Cambridge Press.
- Duncan, J.M., Byrne, P., Wong, K.S. and Mabray, P. (2014), "Stress-strain and bulk modulus parameters for finite element analysis of stress and movements in soil masses", University of California; Berkely, CA, USA.
- Einav, I. (2007), "Beakage mechanics – Part I: Theory", *J. Mech. Phys. Solids.*, **55**(6), 1274-1297.
- Ezaoui, A., Lecompte, T., Di Benedetto, H. and Garcia, E. (2011), "Effects of various loading stress paths on the stress-strain properties and on crushability of an industrial soft granular material", *Granul. Matter.*, **13**(4), 283-301.
- Hardin, B.O. (1985), "Crushing of soil particles", *J. Geotech. Eng.*, **111**(10), 1177-1192.
- Huang, X., Hanley, K.J., O'Sullivan, C., Kwork, C.Y. and Wadee, M.A. (2014), "DEM analysis of the

- influence of the intermediate stress ratio on the critical-state behaviour of granular materials”, *Granul. Matter.*, **16**(5), 641-655.
- Itasca, Consulting Group, Inc. (2008), Particle Flow Code in Three Dimensions (PFC3D); Version 4.0, Itasca, Consulting Group.
- Lade, P.V. and Duncan, J.M. (1975), “Elastoplastic stress–strain theory for cohesionless soil”, *J. Geotech. Engng. Div.*, **101**, 1037-1053.
- Lade, P.V., Yamamuro, J.A. and Bopp, P.A. (1996), “Significance of particle crushing in granular materials”, *J. Geotech. Eng.*, **122**(4), 309-316.
- Matsuoka, H. and Nakai, T. (1978), “A generalized frictional law for soil shear deformation”, *Proceedings of the US–Japan Seminar on Continuum-Mechanical and Statistical Approaches in the Mechanics of Granular Materials*, Tokyo, Japan, pp. 138-154.
- McDowell, G.R. and Bolton, M.D. (1998), “On the micromechanics of crushable aggregates”, *Geotechnique*, **48**(5), 667-579.
- McDowell, G.R. and Harireche, O. (2002a), “Discrete element modeling of soil particle fracture”, *Geotechnique*, **52**(2), 131-135.
- McDowell, G.R. and Harireche, O. (2002b), “Discrete element modeling of yielding and normal compression of sand”, *Geotechnique*, **52**(4), 299-304.
- Nakata, Y., Hyde, A.F.L., Hyodo, M. and Murata, H. (1999), “A probabilistic approach to sand particle crushing in the triaxial test”, *Geotechnique*, **49**(5), 567-583.
- Nakata, Y., Hyodo, M., Hyde, A.F.L., Kato, Y. and Murata, H. (2001a), “Microscopic particle crushing of sand subjected to high pressure one-dimensional compression”, *Soil. Found.*, **41**, 69-82.
- Nakata, Y., Kato, Y., Hyodo, M., Hyde, A.F.L. and Murata, H. (2001b), “One-dimensional compression behaviour of uniformly graded sand related to single particle crushing strength”, *Soil. Found.*, **41**, 39-51.
- Ng, T.-T. (2004), “Shear strength of assemblies of ellipsoidal particles”, *Geotechnique*, **54**(10), 659-669.
- O’Sullivan, C., Wadee, M.A., Hanley, K.J. and Barreto, D. (2013), “Use of DEM and elastic stability analysis to explain the influence of the intermediate principal stress on shear strength”, *Geotechnique*, **63**(15), 1298-1309.
- Randolph, M.F., Dolwin, J. and Beck, R. (1994), “Design of driven piles in sand”, *Geotechnique*, **44**(3), 427-448.
- Robertson, D. (2000), “Numerical simulations of crushable aggregates”, Ph.D. Dissertation, University of Cambridge, UK.
- Sun, D., Huang, W. and Yao, Y. (2008), “An experimental study of failure and softening in sand under three-dimensional stress condition”, *Granul. Matter.*, **10**, 187-195.
- Tarantino, A. and Hyde, A.F.L. (2005), “An experimental investigation of work dissipation in crushable materials”, *Geotechnique*, **55**(8), 575-584.
- Wang, Q. and Lade, P.V. (2006), “Assessment of test data for selection of 3-D failure criterion for sand”, *Int. J. Numer. Anal. Meth. Geomech.*, **30**(4), 307-333.
- Wang, J.F. and Yan, H.B. (2012), “DEM analysis of energy dissipation in crushable soils”, *Soil. Found.*, **52**(4), 644-657.
- Wang, J.F. and Yan, H.B. (2013), “On the role of particle breakage in the shear failure behavior of granular soils by DEM”, *Int. J. Numer. Anal. Meth. Geomech.*, **37**(8), 832-854.
- Weibull, W. (1951), “A statistical distribution function of wide applicability”, *J. Appl. Mech.*, **18**, 293-297.
- Zhou, L.L. and Chu, X.H. (2014), “Evolution of anisotropy in granular materials: Effect of particle rolling and particle crushing”, *Strength. Mater.*, **46**(2), 214-220.
- Zhang, B.Y., Yu, X.J. and Kong, D.Z. (2013), “Particle size distribution and relative breakage for a cement ellipsoid aggregate”, *Comput. Geotech.*, **53**, 31-39.